COMPARISON OF GRID STRATEGIES FOR POINT-DEFECT DIFFUSION SIMULATIONS

G. Punz and K. Dienstl

Siemens AG, PDS, Gudrunstraße 11, A-1100 Wien, Austria

Abstract

A comparison of point-defect simulations on fixed and adaptive grids has been performed. The cases of pure interstitial diffusion, point-defect generation and recombination and coupled point-defect–dopant diffusion are discussed. We find that adaptive grids are much more efficient compared to fixed grids for such simulations.

I. INTRODUCTION

Recently there have been increasing efforts to implement the effects of point-defects in existing process simulators [1], [2]. After choosing a reasonable model the main problem lies in the numerical solution of the differential equations with proper boundary conditions. Severe difficulties arise from the high diffusivities of interstitials and vacancies compared to dopants. Clearly the CPU requirements for such stiff problems depend largely on the discretization schemes in space and time. Due to the vast differences of the diffusivities a single fixed grid, though not equidistant, is not suited for such simulations. To overcome the problem it has been suggested [2] to perform simulations for point-defects and dopants on separate grids, each with a spacing on the order of 0.1 of the diffusion length which may be associated with the respective diffusivity and the simulation time. This certainly may be done in the idealized case where diffusivities will not change over the simulation time and are comparable for interstitials and vacancies. However, if the aim is to simulate real processes - including ramping steps - diffusivities can change drastically. Interstitials and vacancies themselves (or their different charge states) may diffuse vastly different. This would require additional grid separations. Furthermore highly elaborate models (e.g.

with full coupling of dopants, point-defects and structural defects) are being proposed. No simple criterion for setting up a fixed grid may be stated for such cases, and adaptive grids seem very attractive.

In this paper we are concerned with finite-difference spatial discretization and three different time integration schemes as implemented in the simulators ZOMBIE (Gear BDF, [3, 4]), PROMIS (Euler BDF, [4, 3]) and LADIS (Crank Nicholson, [5]). The process simulators ZOMBIE (1d) and PROMIS (2d) apply adaptive grid algorithms to cope with rather general models whereas LADIS uses fixed but not equidistant grids in the current version. Comparative simulations were performed to evaluate the usefulness of adaptive grids. In section II we deal with the simple diffusion of Gaussian point-defect profiles as they result from implantation. The starting profiles were chosen to be quite sharp to represent a stringent test for the numerics of the simulators. Section III discusses surface and bulk generation/recombination. Finally we show the demand for adaptive grids with the example of a coupled diffusion of one dopant and point-defects in section IV.

II. INTERSTITIAL DIFFUSION

To examine the numerical performance of the simulators mentioned above we perform diffusions of Gaussian profiles of interstitials without coupling to vacancies or dopants, i.e. we solve the equation

$$\frac{\partial C_I}{\partial t} = D_I \frac{\partial^2 C_I}{\partial x^2} \tag{1a}$$

with boundary condition

$$\frac{\partial C_I}{\partial x} = 0, \quad (x = 0, \ x = x_b) \tag{1b}$$

The sharpness of the initial distributions ($C_I/C_I^* \sim 10^6$ at the maximum) is not really physical but rather serves as a severe test. The resulting profiles after 6 s, 1 min and 20 min are shown in Fig. 1. We observe a very good agreement over several decades of the time and concentration range. Although the 2d simulators LADIS and PROMIS were run in their 1d mode the purely 1d program ZOMBIE is clearly superior. (It is to note that although LADIS uses a fixed grid the simulation is extended only as deep into the bulk as necessary for a given time.) Calculations on a fixed grid show decreasing convergence properties with simulation time: since a certain number of grid lines is necessary to resolve the

initial profile this forces a coarser grid deeper in the bulk. Using more gridlines on the whole is not really an alternative, as all lines remain in the simulation region, even if the profiles flatten out. We stress that for realistic diffusion times setting up a fixed grid with an appropriate resolution of the profile for all simulation times is not feasible. This is obvious from Fig. 2 which shows the adaptation of the spatial grid of PROMIS during diffusion. An equally well suited fixed grid would have to include all shown grid lines.

Table 1 summarizes CPU demands and time steps. The numbers of time steps are not directly comparable between the different integration schemes. We note that the adaptation of the grid during the early stages of the diffusion allows much longer time steps later on, therefore reducing the overall CPU time.

In two dimensions an optimal grid control is even more important because of the severe limitations on the number of gridpoints. We have performed the analogous calculations after implanting an interstitial profile near a mask edge. In Fig. 3 we show the initial, an intermediate and the final state of the adaptive grid as generated by PROMIS.

III. POINT-DEFECT GENERATION/RECOMBINATION

We now turn to a more physical situation where both interstitials and vacancies are present and at nonequilibrium concentrations. It is well known that during oxidation interstitials are generated at the oxide-silicon boundary. Further the recombination of interstitial-vacancy pairs in the bulk has to be taken into account. We neglect the moving boundary as its effect with regard to changes in the point-defect distributions is small compared to the generation/recombination terms. The one-dimensional model is described by the following equations ([2]):

$$\frac{\partial C_I}{\partial t} = D_I \frac{\partial^2 C_I}{\partial x^2} - K_{IV}\left(C_I C_V - C_I^* C_V^*\right) \tag{2a}$$

$$\frac{\partial C_V}{\partial t} = D_V \frac{\partial^2 C_V}{\partial x^2} - K_{IV}\left(C_I C_V - C_I^* C_V^*\right) \tag{2b}$$

and the boundary conditions at the surface

$$D_I \frac{\partial C_I}{\partial x} = g_I^{surf}(t) - K_I\left(C_I - C_I^*\right) \tag{2c}$$

$$D_V \frac{\partial C_V}{\partial x} = -K_V (C_V - C_V^*) \qquad (2d)$$

K_{IV} is the bulk recombination velocity of interstitial-vacancy pairs, K_I and K_V are the velocities for surface recombination of interstitials and vacancies. The interstitial surface generation rate g_I^{surf} may be time dependent e.g. according to a Deal-Grove law but is assumed to be constant in our case. Most of the parameters of Eqs. 2a-d are not well known, the values found in literature spread by some orders of magnitude.

Fig. 4 presents the simulation of Eqs. 2a-d by ZOMBIE for the set of parameters ([6], unless stated):

$$C_I^* = 5 \cdot 10^{22} \cdot exp(-1.82eV/k_B T)/cm^3,$$
$$C_V^* = C_I^*,$$
$$D_I = 914 \cdot 10^{-4} \cdot exp(-3.02eV/k_B T) \, cm^2/s,$$
$$D_V = 0.6 \cdot 10^{-4} \cdot exp(-2.21eV/k_B T) \, cm^2/s,$$
$$K_I = 6.01 \cdot 10^{-13} \cdot exp(+1.58eV/k_B T) \, cm/s \, [2],$$
$$K_V = 3 \cdot 10^{-7} cm/s,$$
$$K_{IV} = 10^{-17} cm^3/s$$

and
$$g_I^{surf} = 10^{11}/cm^2 s \text{ (this work)}$$

for T=1173 K on a logarithmic depth scale. Table 2 compares CPU demands for fixed and adaptive grids. Again the latter is clearly more efficient. For a fixed grid calculation the costs are excessive for longer simulation times. This is also obvious from a look to the adaptive grid (which is not shown here): for the first few seconds most of the grid lines are needed at the surface. Afterwards they are moved by the gradients of interstitial and vacancy concentrations deeper into the bulk.

IV. COUPLED DOPANT - POINT-DEFECT DIFFUSION

We supplement now our calculations with simulations of the coupled diffusion of a dopant with point-defects. It is known that Boron diffusivity is enhanced for short annealing steps after implantation [7], but in general the short time diffusion properties of dopants are not well understood. As an illustrative example with regard to grid adaptation we performed diffusions of a phosporus profile implanted at 200 KeV and interstitials and vacancies profiles corresponding to a phosphorus implantation at 300 KeV and 100 KeV, respectively. This should represent roughly the main features of damage profiles, but the details are not important here.

One equation for the dopant has to be added to eqs. 2a,b and 2c,d:

$$\frac{\partial C_D}{\partial t} = D_D \frac{\partial^2 C_D}{\partial x^2} \tag{3a}$$

$$\frac{\partial C_D}{\partial t} = 0, \quad (x = 0, \ x = x_b) \tag{3b}$$

with a dependence of the diffusion coefficient of phosphorus on the local point-defect concentration [8], [9]:

$$D_D = D_D^0 \cdot \left[f \frac{C_I}{C_I^*} + (1 - f) \frac{C_V}{C_V^*} \right] \tag{3c}$$

For f we take the values given by Fahey [10]. Further, as we simulate solely the effect of point-defects resulting from implantation damage, we set g_I^{surf} to zero.

Fig. 5 depicts the change of the dopant and point-defect concentrations during a 1 minute annealing at 1223 K for the parameter set given above (simulation by ZOMBIE). Phosphorus diffusion is not significantly enhanced because the point-defects concentrations are near equilibrium after a few seconds. To show the sensitivity with respect to parameters we perform the same simulation with the diffusivities of point defects reduced by a factor of 10. It is seen that the phosphorus profile moves deeper into the bulk because the enhancement produced by interstitial supersaturation is effective for a longer time. From the resulting profiles we note drastic changes in their gradients which of course have to be reflected in the simulation grids. Any a priori setup of a fixed grid will be questionable.

At this point we are not aware of a consistent parameter set for the short time annealing of dopant implantation damage. Further simulations with varying parameters and comparisons with experiments are needed. However, it is clear that only adaptive grids enable an efficient way to perform such simulations.

V. CONCLUSION

We performed simulations of point-defect diffusion with different simulators on three levels of complexity. Comparing fixed and adaptive grid algorithms we find that for diffusion times of typical IC-fabrication processes and for more complex diffusion models grid adaptation is mandatory.

References

[1]   D. Collard and K. Taniguchi: " IMPACT- A Point-Defect-Based
       Two-dimensional Process Simulator: Modeling...", *IEEE Trans.
       Electron Devices*, vol. ED-33, no. 10, pp. 1454-1462, Oct. 1986

[2]   M.R. Kump and R.W. Dutton: "The Efficient Simulation of
       Coupled Point Defect and Impurity Diffusion", *IEEE Trans.
       Computer-aided Design*, vol. CAD-7, no. 2, pp. 191-204, Feb.
       1988

[3]   W. Jüngling, P. Pichler, S. Selberherr, E. Guerrero, H. Pötzl:
       "Simulation of Critical IC-Fabrication Processes Using Advanced
       Physical and Numerical Methods", *IEEE J. Solid-State Circuits*,
       Joint Special Issue on VLSI, vol. SC-20, no. 1, pp. 76-87, Feb.
       1985

[4]   P. Pichler, W. Jüngling, S. Selberherr, E. Guerrero, H. Pötzl: "Si-
       mulation of Critical IC-Fabrication Steps", IEEE Trans. Electron
       Devices, Joint Special Issue on Numerical Simulation of VLSI, vol.
       ED-32, no. 10, pp. 1940-1953, Oct. 1985

[5]   R. Tielert: "Two-dimensional numerical analysis of doping pro-
       cesses", Proc. of NASECODE III Conference (Galway 1983), ed.
       by J.J.H. Miller, Boole Press, 1983

[6]   M. Budil: Proc. of NUMOS I Conference (Los Angeles 1986), ed.
       by J.J.H. Miller, Boole Press, 1987, and private communication

[7]   K. Cho, M. Numan, T.G. Finstad, W.K. Chu, J. Liu, J.J. Wortman:
       "Transient enhanced diffusion during rapid thermal annealing of
       boron implanted silicon", *Appl. Phys. Lett.* , vol. 47, no. 12, pp.
       1321-1323, 1985

[8]   S.M. Hu: "Formation of stacking faults and enhanced diffusion of
       phosphorus in the oxidation of silicon", *J. Appl. Phys.*,vol. 45, pp.
       1567-1573, 1974

[9]   D.A. Antoniadis: "Oxidation induced point-defects in silicon", *J.
       Electrochem. Soc.*, vol. 129, pp. 1093-1097, 1982

[10]   P.M. Fahey: "Point Defects and Dopant Diffusion in Silicon", PhD
       Dissertation, Dep. of Electrical Engineering, Stanford University,
       June 1985

Acknowledgement
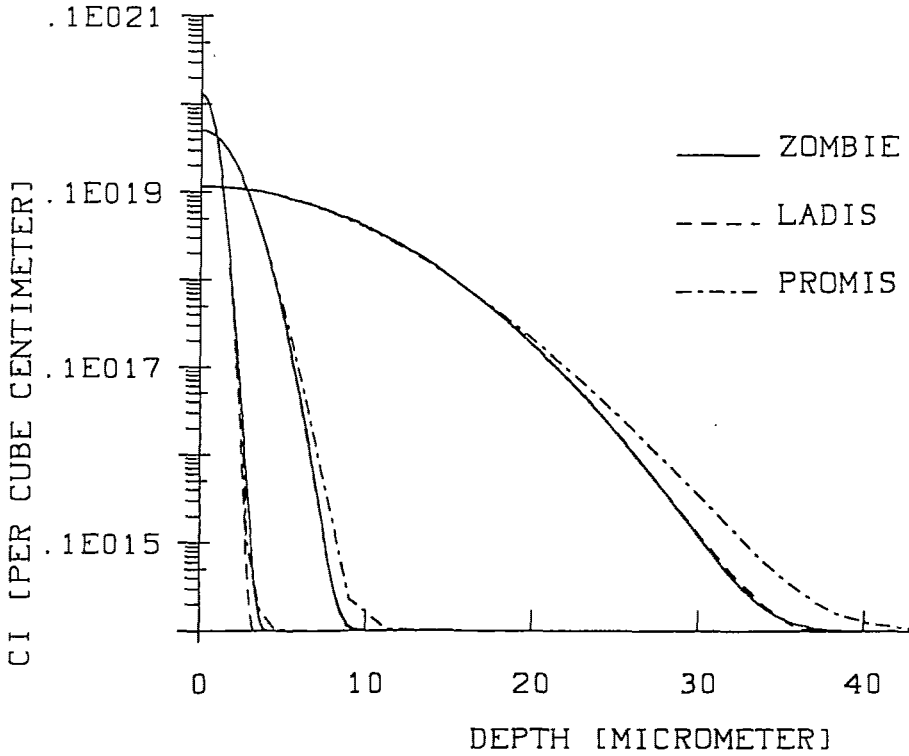
Fig. 1: Diffused interstitial profiles as calculated by different simulators (1273 K; after 6 s, 1 min and 20 min). Implantation parameters: Gaussian, 0.35 μ projected range, 0.077 μ standard deviation, $1 \cdot 10^{15}/cm^3$ dosis. $D_I = 3.65 \cdot 10^{-4}\ exp(-1.58eV/k_B T)\ cm^2/s$ [2].

grid	ZOMBIE		LADIS	PROMIS
	fixed	adaptive	fixed	adaptive
(maximal) number of lines	101	162	162	162
time steps until				
6 s	27	27	288	36
1 min diffusion	61	59	687	55
20 min	197	114	5511	92
MFLOP's until				
6 s	3,6	9,2	85	200
1 min diffusion	12,8	22,5	340	308
20 min	145	47	2616	472

Table 1: Performance of simulators (1d interstitial simulation)
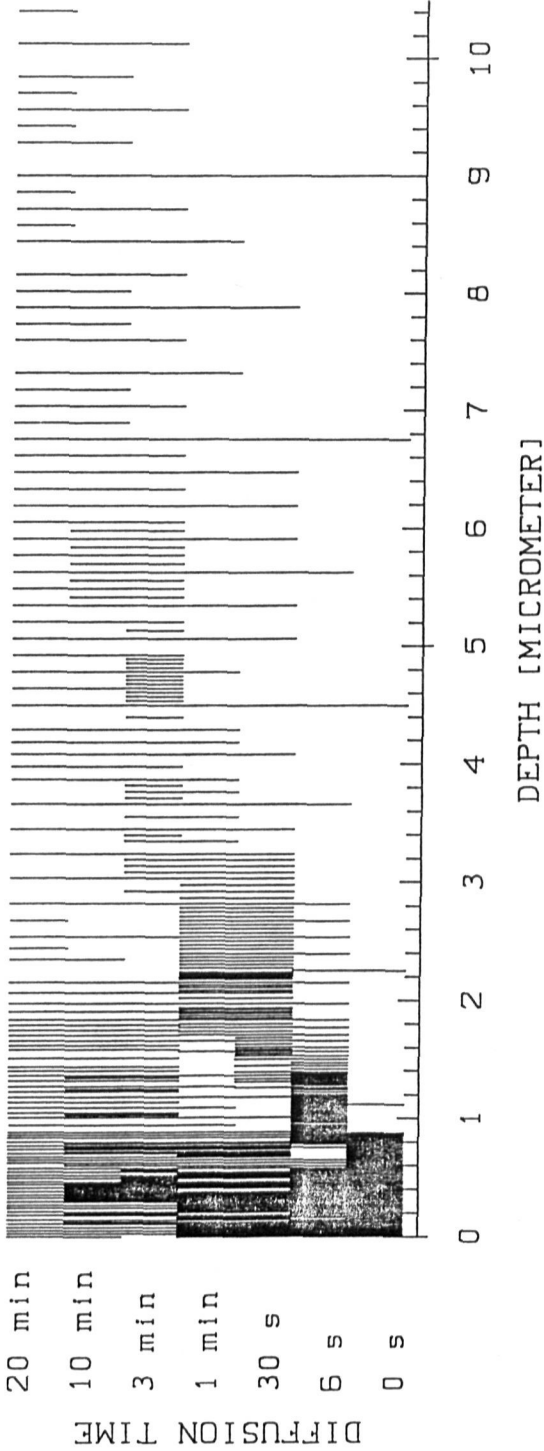
Fig. 2: Evolution of adaptive grid during interstitial diffusion (simulation by PROMIS). For diffusion times and parameters see Fig. 1. (Regions of highest grid density cannot be resolved on this plot.)
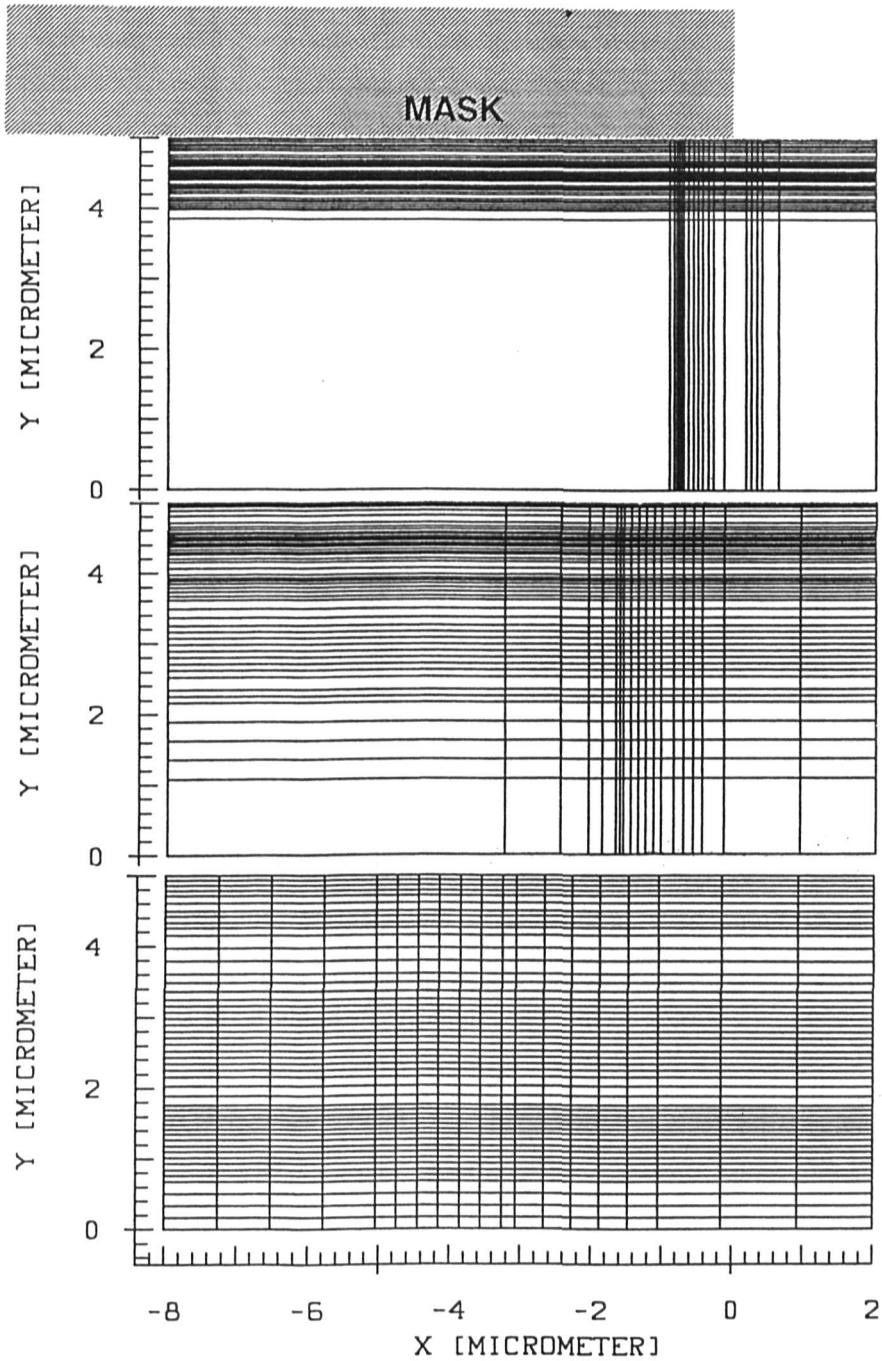
Fig. 3: Evolution of a 2d adaptive grid during interstitial diffusion as simulated by PROMIS (1273 K; after implantation, 4.8 s and 76.2 s diffusion). Implantation parameters: Gaussian, 0.53 μ projected range, 0.092 μ standard deviation, $5 \cdot 10^{15}/cm^3$ dosis.
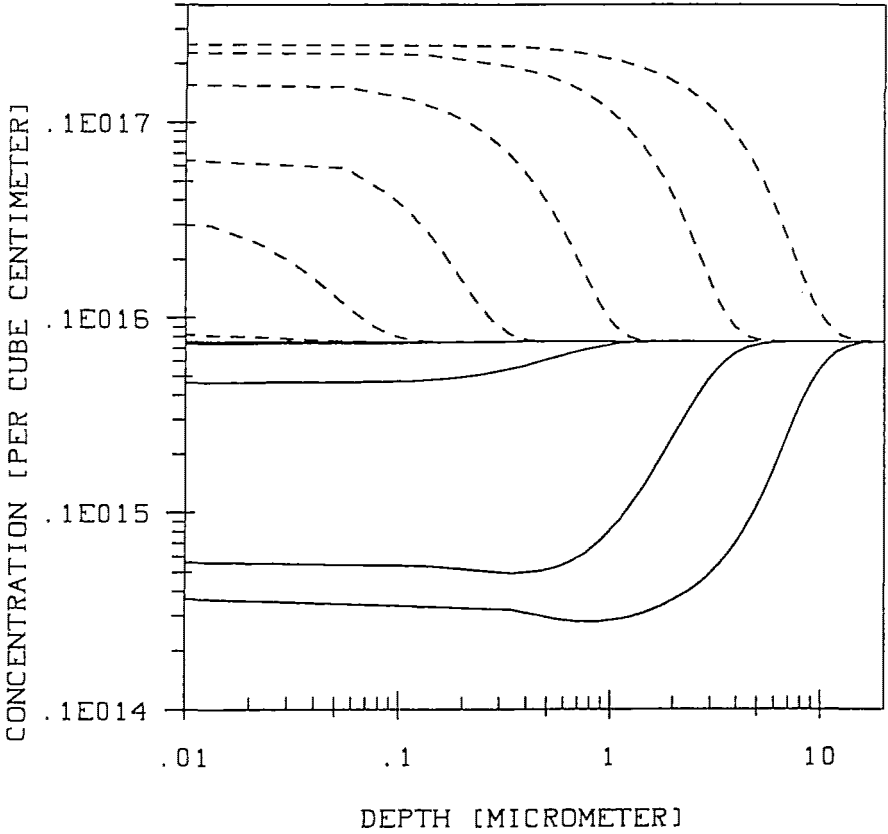
Fig. 4: Point-defect simulation including interstitial surface generation and surface and bulk recombination. Vacancy (full line) and interstitial (dashed line) profiles are shown after 0.01 s, 0.1 s, 1 s, 10 s, 120 s and 900 s. (Vacancy profiles are indistinguishable from the equilibrium concentration up to 1 s.)

diffusion time	fixed grid	adaptive grid
0.001 s	15.88	4.98
0.01 s	40.3	14.4
0.1 s	87.6	47.0
1. s	319	91
10 s	1728	197
120 s	-	734
900 s	-	3069

Table 2: CPU costs for point-defect diffusion simulation in arbitrary units (1173 K, simulation by ZOMBIE).
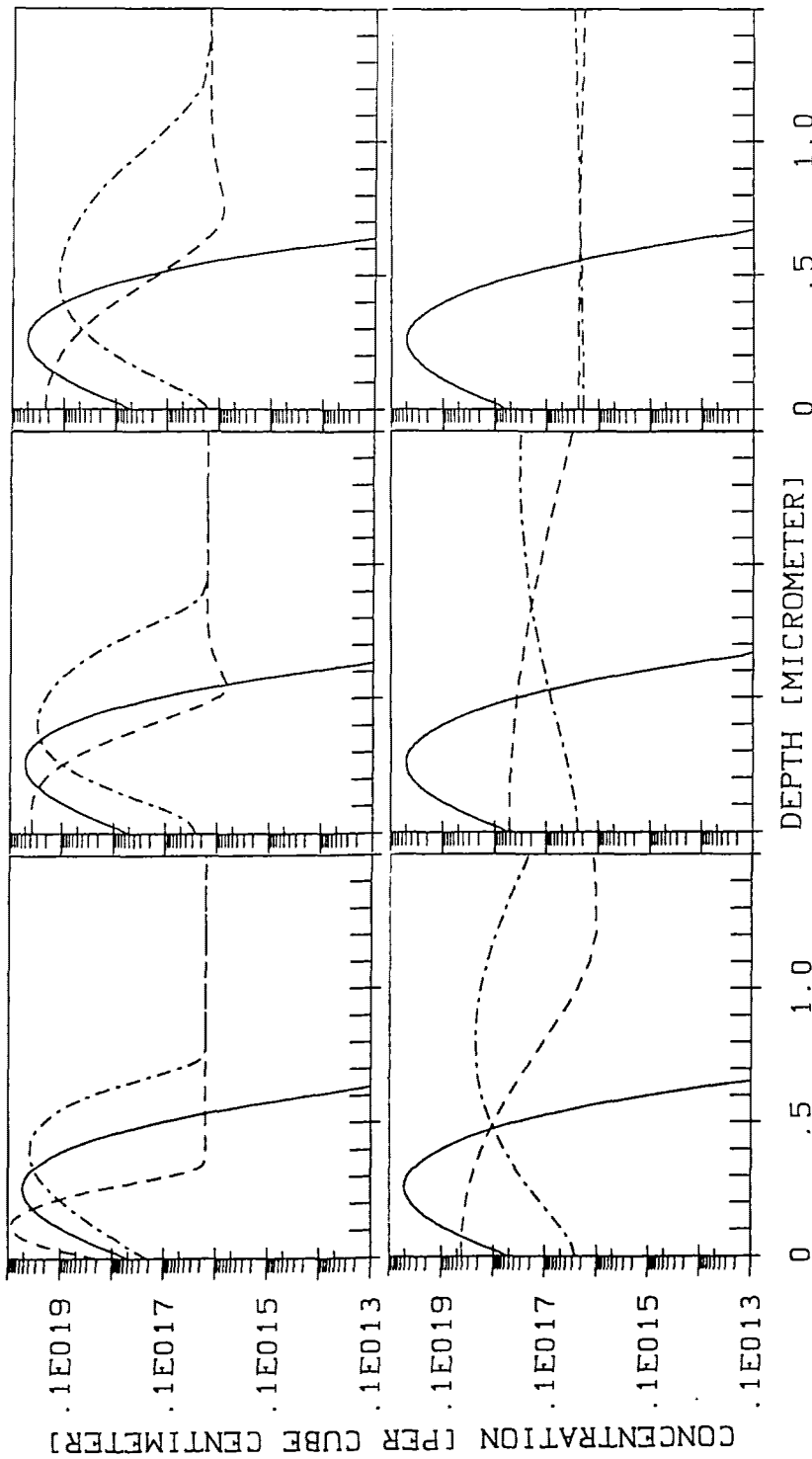
Fig. 5: Short time annealing of phosphorus (full) with vacancies (dashed) and interstitials (dot-dashed line). Plots are after implantation and at 0.1 s, 0.5 s, 2.5 s 10s and 1 min.

428
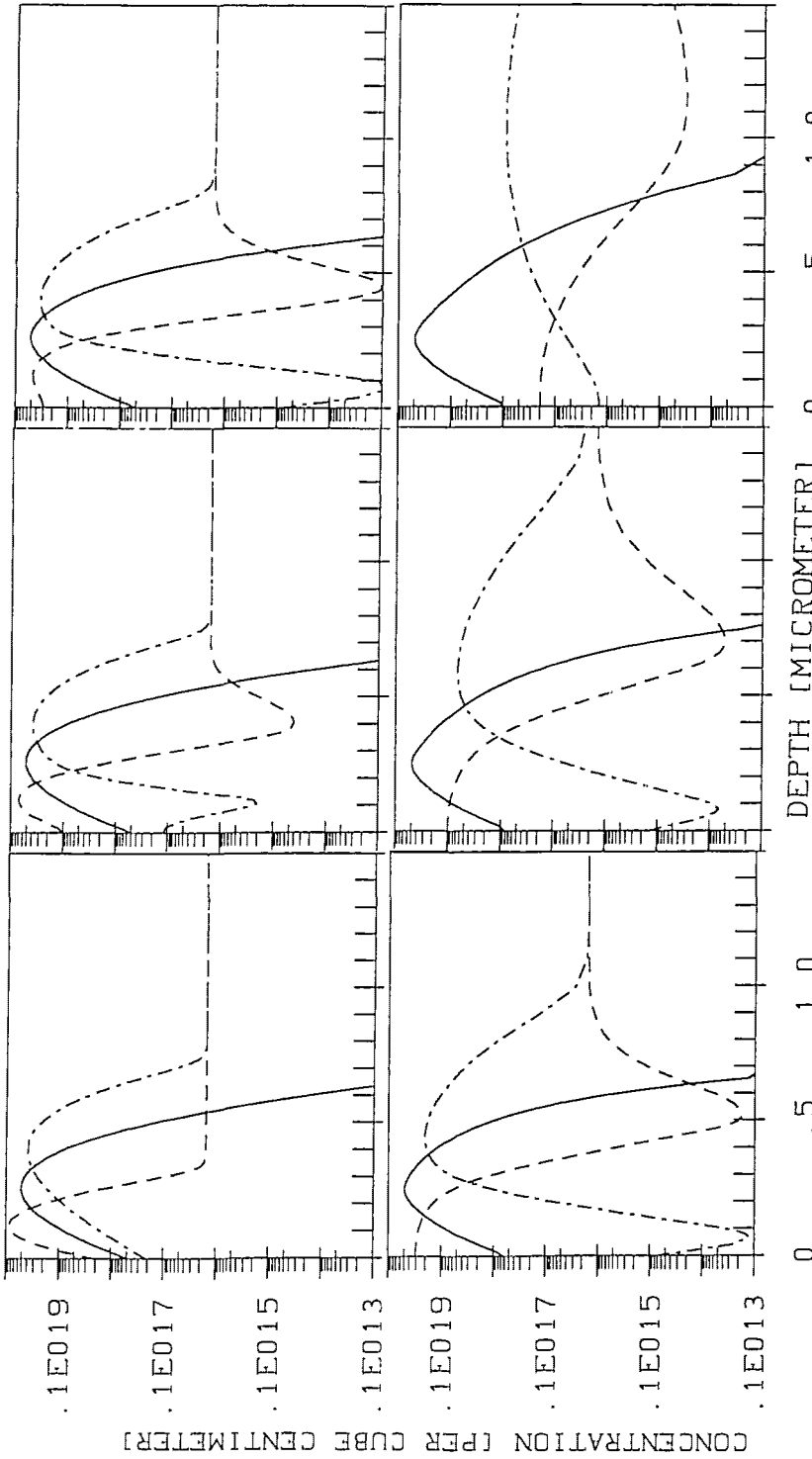
Fig. 6: Same as Fig. 5, but with lower D_I and D_V (see text). Plots are after implantation and at 0.1 s, 0.5 s, 2.5 s 10s and 1 min.

DEPTH [MICROMETER]

CONCENTRATION [PER CUBE CENTIMETER]